ChemBioChem

Research Article
doi.org/10.1002/cbic.202400020

Chemistry Europe
European Chemical Societies Publishing

www.chembiochem.org

Binding Dynamics of a Stapled Peptide Targeting the Transcription Factor NF–Y

Canan Durukan,[a, b] Federica Arbore,[a, b] Rasmus Klintrot,[a, b] Carlo Bigiotti,[c, d] Ioana M. Ilie,[c, d] Jocelyne Vreede,[c, d] Tom N. Grossmann,*[a, b] and Sven Hennig*[a, b]

Transcription factors (TFs) play a central role in gene regulation, and their malfunction can result in a plethora of severe diseases. TFs are therefore interesting therapeutic targets, but their involvement in protein–protein interaction networks and the frequent lack of well–defined binding pockets render them challenging targets for classical small molecules. As an alternative, peptide–based scaffolds have proven useful, in particular with an α-helical active conformation. Peptide–based strategies often require extensive structural optimization efforts, which could benefit from a more detailed understanding of the dynamics in inhibitor/protein interactions. In this study, we investigate how truncated stapled α-helical peptides interact with the transcription factor Nuclear Factor-Y (NF–Y). We identified a 13-mer minimal binding core region, for which two crystal structures with an altered C-terminal peptide conformation when bound to NF–Y were obtained. Subsequent molecular dynamics simulations confirmed that the C-terminal part of the stapled peptide is indeed relatively flexible while still showing defined interactions with NF–Y. Our findings highlight the importance of flexibility in the bound state of peptides, which can contribute to overall binding affinity.

Introduction

Transcription factors (TFs) play a critical role in gene regulation.[1] They bind to specific DNA sequences and initiate transcription for specific subsets of genes.[2] TFs can function independently or in complex with other proteins. Disruption or dysregulation of TFs, including the assembly of their complexes, can lead to a wide range of abnormalities and diseases including cardiovascular diseases,[3] asthma and allergies,[4] as well as Alzheimer's disease,[5] multiple sclerosis and many forms of cancer.[6] Therefore, TFs represent a promising group of therapeutic targets, but are often regarded as challenging due to their involvement in complex protein-protein interaction (PPI) networks, and the frequent absence of well-defined binding pockets. Typical intervention strategies involve the modulation of the dynamic interaction networks.[7]

For such challenging targets, peptide–derived scaffolds provided potent interaction inhibitors.[8] Here, in particular, the α-helical motif which is commonly found at protein–protein interfaces has drawn considerable attention.[9] A preorganization of the helical conformation can lead to a reduction of entropic penalty upon binding and therefore increase binding affinities.[10] Hydrocarbon peptide stapling is often used for that purpose, combining two α-helix stabilization methods: α,α-disubstitution and the formation of a macrocyclic bridge.[11] In this setup, the macrocycle is mostly formed between *i*,*i*+4 or *i*,*i*+7.[11b,c] Although, stapled peptides have provided active TF modulators,[12] a more detailed understanding of their dynamic interaction with TFs can further support the design process.

Previously, we reported stapled peptide inhibitors of the transcription factor, nuclear factor Y (NF–Y), which plays an important role in the regulation of metabolic pathways which are crucial for cancer cells.[13] E.g., NF–Y has been described to be overexpressed in breast and gastric cancer.[14] However, only a very limited set of tool compounds is available to study this transcription factor.[12b] Notably, NF–Y comprises a protein complex that involves three highly conserved subunits: A, B, and C. Only the intact NF–Y complex can bind to the target DNA CCAAT box, a common element found within eukaryotic promoters.[15] Subunits B and C form a stable heterodimeric complex,[15] and are fundamental for the functionality of NF–Y.[16] They exhibit a weak and sequence independent affinity for double stranded–DNA, but do not activate gene transcription without the third component NF–YA. NF–YA, binds to the CCAAT box in a sequence-specific manner, however only with sufficient affinity when bound to the NF–YB/C

[a] C. Durukan, F. Arbore, R. Klintrot, Prof. Dr. T. N. Grossmann, Dr. S. Hennig
Department of Chemistry and Pharmaceutical Sciences
VU University Amsterdam
De Boelelaan 1108, 1081 HZ, Amsterdam, The Netherlands
E-mail: t.n.grossmann@vu.nl
s.hennig@vu.nl

[b] C. Durukan, F. Arbore, R. Klintrot, Prof. Dr. T. N. Grossmann, Dr. S. Hennig
Amsterdam Institute of Molecular and Life Sciences (AIMMS)
VU University Amsterdam
De Boelelaan 1108, 1081 HZ, Amsterdam, The Netherlands

[c] C. Bigiotti, Dr. I. M. Ilie, Dr. J. Vreede
Van't Hoff Institute for Molecular Sciences
University of Amsterdam
Science Park 904, 1098 XH Amsterdam, The Netherlands

[d] C. Bigiotti, Dr. I. M. Ilie, Dr. J. Vreede
Amsterdam Center for Multiscale Modeling (ACMM)
University of Amsterdam
P.O. Box 94157, 1090 GD Amsterdam, The Netherlands

Supporting information for this article is available on the WWW under https://doi.org/10.1002/cbic.202400020

heterodimer.[17] Trimer formation is mediated via predominantly positively charged residues of NF–YA binding to a negatively charged binding patch on NF–YB/C.[15,18]

Earlier, we have described the stapled peptide **2D^N** which targets the NF–YB/C heterodimer and prevents NF–YA binding.[12b] Herein, we report a set of **2D^N**-derived stapled peptides with reduced sequences length and their structural characterization. We identified a minimal core binding scaffold comprising a 13-mer sequence. Biochemical, structural as well as computational studies revealed varying binding dynamics within different regions of the sequence, highlighted by two distanced crystal structures. Overall, we miniaturized a NF–YB/C binding peptide and shed light on the different binding dynamics of a stably bound N-terminus compared to a flexible C-terminal end.

Results and Discussion

NF–YB/C Dimer is Pure, Monodisperse and Functional

For protein crystallography, protein purity is important. In addition, monodispersity is essential, in particular, when working with protein complexes. The NF–YB/C heterodimer (Supporting Figure S1) was polycistronically expressed and co-purified, using a His_6-affinity tag fused to the NF–YB subunit. The quality of the resulting protein was assessed using SDS–PAGE (Supporting Figure S2). Notably, the NF-YB and NF–YC subunits were found to co–migrate in one clean band, as their molecular weight difference of 379 Da could not be resolved with the SDS–PAGE gel. To identify each individual subunit, we performed HPLC ESI MS ensuring the presence of an intact heterodimer (Supporting Figure S3, Supporting Table S1). The structural integrity of the NF–YB/C heterodimer was validated via analytical size exclusion chromatography (SEC), resulting in one apparent species in solution eluting in a single sharp peak at 12.1 mL (Figure 1A).

Calibration (Supporting Figure S4) against protein standards shows that the heterodimer eluted between ovalbumin (MW = 43 kDa, 13.6 mL) and albumin (MW = 66.5 kDa, 11.0 mL), which makes it appear slightly bigger than its calculated molecular weight ($MW_{NF–YB/C}$ = 22.1 kDa). This is presumably due to its oval shape observed in the crystal structure (Supporting Figure S1).

We verified the oligomeric state of the NF–YB/C complex as a heterodimer using Dynamic Light Scattering (DLS) analysis (Figure 1B). The data revealed a single peak, showing an apparent hydrodynamic radius (r_H = 2.42 nm), corresponding to an estimated diameter of approximately 4.8 nm which is in line with our earlier structural analysis (Supporting Figure 1, size: 3.0×5.3 nm). This consistency between experimental DLS results and crystallography data substantiates the NF–YB/C complex as a highly uniform heterodimer with a polydispersity index (*PDI*) of 0.13, falling within the expected size range. Importantly, our DLS analysis indicated the absence of any higher oligomeric species in the solution, reaffirming the monodisperse nature of the NF–YB/C complex.

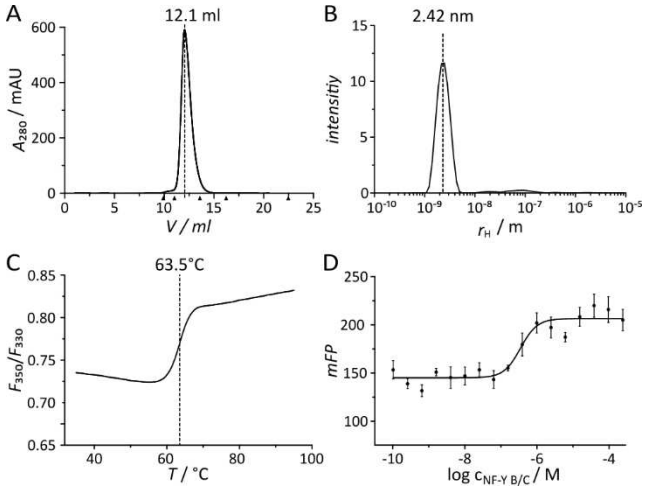

Figure 1. A) Analytical SEC of NF–YB/C was performed on a 10/300 S75 column (Äkta Pure, Cytiva) and shows a single species in solution eluting with an elution volume of 12.1 mL. Elution volumes of relevant calibration proteins are indicated by arrowheads (Supporting Figure S4). B) DLS (Prometheus Panta, Nanotemper) revealed the distribution of hydrodynamic radii, showing a single peak at 2.42 nm and a PDI of 0.13. C) NanoDSF (Prometheus Panta, Nanotemper) was performed using the ratio of the quenching of intrinsic tryptophan fluorescence (F_{350}/F_{330} ratio). The inflection point indicates the melting point of the NF–YB/C complex (T_m = 63.5 °C, see also the analysis of the first derivative *f*′(T), Supporting Figure S5). D) Direct binding of NF–YB/C to **2D^N** in an FP assay. Sigmoidal curve could be fitted to a $K_D = 0.35 \pm 0.10$ μM. All values are mean values of triplicates, and error margins are given as standard deviations.

To assess the stability of the heterodimer, we subjected it to thermal denaturation experiments using nano differential scanning Fluorimetry (nanoDSF). Quenching of intrinsic tryptophane fluorescence (λ_{Em} = 350 nm) upon unfolding and Trp exposure to the aqueous buffer environment was used as a measure of protein unfolding. The resulting sigmoidal curve shape (Figure 1C) characteristic of thermal unfolding provided a melting temperature (T_m) of 63.5 °C. Hence, it confirmed the stability and robustness of the NF–YB/C heterodimer in solution.

In addition to its structural integrity and stability, we tested if the NF–YB/C heterodimer is functional by binding to a previously reported NF–YA derived binder **2D^N**. Hydrocarbon stapled peptide **2D^N** harbors an *i*,*i*+4 crosslink but lacks one of the characteristic Cα-methyl groups to allow adoption of a particular N-terminal configuration (Supporting Figure S6).[12b] In a fluorescence polarization (FP) assay, NF–YB/C heterodimer was titrated against a fluorescently labeled version of **2D^N** (Figure 1D, Supporting Figure S7) to provide a binding affinity ($K_D = 0.35 \pm 0.10$ μM) consistent with previous reports.

Taken together, we could show that the NF–Y subunits B and C form a compact and stable heterodimer with a uniform particle size and little to no other species in solution. The heterodimer is functional as it binds the NF–YA derived peptide **2D^N** with an expected affinity. This provides an excellent starting point for further biophysical characterization of peptide–derived binders.

Truncated Sequences Benefit More from Stapling

Given the importance of polar interactions for peptide binding to NF–YB/C,[17] we were interested how a variation of salt concentration affects binding affinity. Consequently, FP assays of FITC labelled **2D^N** were performed under different salt concentrations. Higher concentrations of NaCl led to a decrease of the apparent binding affinity (Figure 2A), presumably due to the competition of salt ions with the peptide for binding. However, low salt concentrations ($c < 250$ mM) caused NF–YB/C to precipitate, when not bound to a peptide ligand. We concluded to use a salt concentration of 250 mM NaCl for subsequent assays.

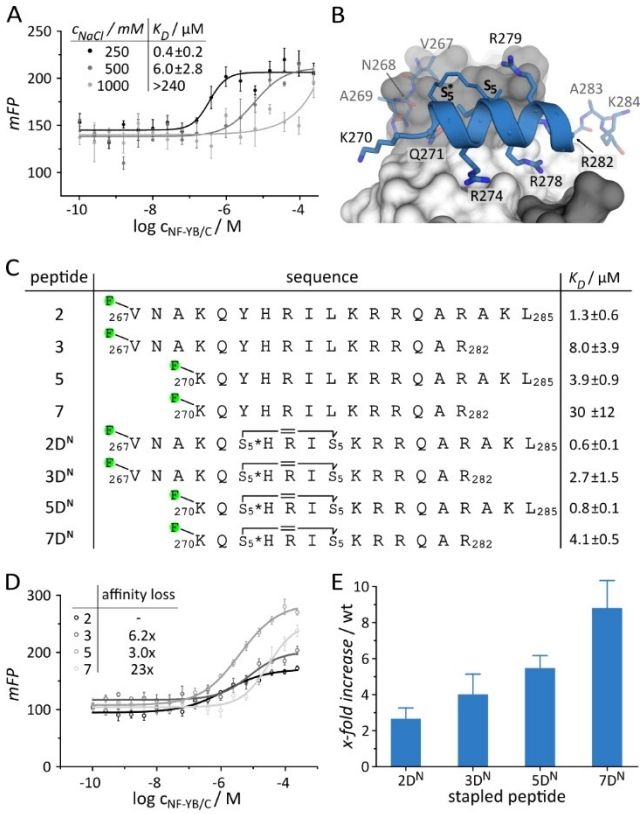

Figure 2. A) Binding of **2D^N** to NF–YB/C was analyzed using various NaCl concentrations to evaluate the influence of salt on the apparent binding affinity. A FITC fluorophore is attached to the N-terminus of **2D^N** via a PEG2 linker. All K_D-values are summarized in the inlay and are mean values of triplicates, error margins are given as standard deviations. B) Crystal structure (PDB ID 6qmq) of NF–YB/C (light–grey and dark grey surface representation) in complex with **2D^N** (blue helix and stick representation).[12b] Peptide amino acids are labelled in single letter code and numbered according to NF–YA nomenclature. Hydrocarbon stapling positions are indicated as **S$_5$*** and **S$_5$**. L285 is not visible in electron density and therefore also not visible in the model. C) Design of truncated peptide panel. **S$_5$*** and **S$_5$** were used for peptide stapling ($i,i+4$) using ring closing metathesis (black lines indicate hydrocarbon staple, = indicates double bond after ring closing metathesis). **S$_5$***:(S)-2-(4-pentenyl)glycine, **S$_5$**: (S)-2-(4-pentenyl)alanine. For subsequent FP assays a FITC fluorophore is attached to the N-terminus of all peptides via a PEG2 linker (green sphere). D) Direct binding of NF–YB/C to the indicated panel of non-stapled peptide (N-terminally FITC labelled via a PEG2 linker) truncations using the FP assay. Sigmoidal curves were fitted to the affinities. All K_D-values are mean values of triplicates. Error margins are given as standard deviations. E) Affinity increase in x-fold change of stapled peptide truncations compared to their unstapled counterparts (wt). For FP assays peptides were N-terminally FITC labelled via a PEG2 linker. For raw data titrations, see supplementary information (Figure S8).

To further explore the binding contributions of the different peptide regions to NF–Y B/C binding, we designed a set of FITC-labelled peptides with N- and C-terminal truncations. This was based on the crystal structure of **2D^N** bound to NF–YB/C (Figure 2B). We noted that the side chains of V267, N268, and A269 do appear not to engage in direct interactions, while K270 plays a vital role in contacting the NF–YB/C binding groove (Figure 2B). At the C terminus, amino acids A283 and K284 are again not directly participating in binding, with C-terminal L285 displaying considerable flexibility (not resolved in the crystal structure, PDB ID 6qmq, Figure 2B).[12b] On the other hand, R282 had a direct connection with the binding surface, making it essential to retain.

Based on these observations, we designed a peptide panel with N-terminal and/or C-terminal truncations (Figure 2C). Among the panel, the shortest peptide (**7**) comprised only 13 amino acids, spanning from K270 to R282. Initially, non–stapled peptides (**2**, **3**, **5**, **7**) were synthesized and tested in an FP assay with NF–YB/C. Peptide **2** showed the highest binding affinity ($K_D = 1.3 \pm 0.6$ µM) with all other peptides following with decreasing affinities in the order of **5** > **3** > **7** (Figure 2D). Notably, shortening the sequence on the C-terminus resulted in more severe affinity losses (6.2-fold reduced compared to **2**) than N-terminal truncation (3.0-fold reduced compared to **2**). N- and C-terminally truncated peptide **7** experienced the most severe affinity loss (23-fold reduced compared to **2**).

We also investigated the impact of hydrocarbon stapling on the binding affinities of these FITC-labelled peptides utilizing the previously reported stapling architecture (in analogy to **2D^N**, Supporting Figure S6) .[12b] Notably, all stapled peptides (Figure 2C) show increased binding affinity when compared to their unmodified counterparts, with the affinity enhancement increasing upon sequence truncations (Figure 2E): from 2.2-fold (**2**→**2D^N**) to 7.3-fold (**7**→**7D^N**). As a consequence, the stapled peptides suffer less from truncations. E.g., **5D^N**, which had a 3-amino acid truncation at the N-terminus (VNA), showed an affinity close to that of the original best binder, **2D^N** ($K_D = 0.8 \pm 0.1$ µM compared to $K_D = 0.6 \pm 0.1$ µM for **2D^N**, Figure S8 for comparison). Most notably, **7D^N**, despite undergoing truncations at both termini, exhibited a considerable binding affinity ($K_D = 4.1 \pm 0.5$ µM).

7D^N Adopts Differential Poses when Bound to NF–YB/C

To validate the binding modes of the peptide binders to the NF–YB/C heterodimer, we crystallized the complexes and solved their atomic structures via X-Ray Diffraction (XRD, PDB ID 8qu2) starting with **5D^N**. The complex formed rod–shaped crystals measuring approximately 20×30×50 µm within the space group $P2_12_12_1$ (#19). Data up to a resolution of 1.45 Å was taken into account during integration using XDS[19] (Table 1). Utilizing the NF–YB/C heterodimer (PDB ID 6qmp, chain B&C) as a search model for molecular replacement (Phaser),[20] the structure was solved, unveiling one heterodimer per asymmetric unit. Within

Table 1. Crystallographic table of the data collection and refinement data of the crystal structures of NF–YB/C in complex with peptide **5D^N** (PDB ID 8qu2), **7D^N**_IN (PDB ID 8qu3) and **7D^N**_OUT (PDB ID 8qu4). Values in parenthesis correspond to the highest resolution shell.

Structure	NF–YB/C:**5D^N** (PDB ID: 8qu2)	NF–YB/C:**7D^N**_IN (PDB ID: 8qu3)	NF-YB/C:**7D^N**_OUT (PDB ID: 8qu4)
Data collection	DLS, I04	DLS, I04	DLS, I04
detector	DECTRIS EIGER 2×16 M	DECTRIS EIGER 2×16 M	DECTRIS EIGER 2×16 M
wavelength (Å)	0.9537 Å	0.9537 Å	0.9537 Å
resolution limits (Å)	19.86–1.45 (1.50–1.45)	41.94–1.41 (1.46–1.41)	41.82–1.38 (1.43–1.38)
space group (#)	$P2_12_12_1$ (19)	$P2_12_12_1$ (19)	$P2_12_12_1$ (19)
cell dimensions			
a, b, c (Å)	45.08, 51.46, 72.55	44.75, 51.39, 72.56	44.45, 51.40, 71.91
α, β, γ (°)	90.0, 90.0, 90.0	90.0, 90.0, 90.0	90.0, 90.0, 90.0
# total reflections	405265 (38947)	765317 (59431)	801137 (69853)
# unique reflections	30609 (3024)	30830 (2923)	32648 (3329)
multiplicity	13.2 (12.9)	24.8 (20.3)	24.5 (20.6)
completeness (%)	99.90 (99.83)	93.44 (89.90)	94.69 (98.14)
$I/\sigma I$	25.42 (2.89)	26.10 (1.60)	28.52 (1.76)
$CC_{1/2}$	1 (0.911)	1 (0.747)	1 (0.784)
R_{meas}	0.05476 (0.7769)	0.06265 (1.835)	0.05526 (1.378)
Refinement			
# total reflections	30595 (3019)	30817 (2921)	32587 (3329)
# reflections R_{free}	1573 (138)	1518 (132)	1596 (154)
R_{work}/R_{free}	0.1405 / 0.1718	0.1655 / 0.1992	0.1698 / 0.2132
# atoms (non–hydrogen)	1765	1717	1648
protein	1471	1454	1422
peptide	133	124	124
ligands/ions	22	11	12
water	139	128	90
protein residues	183	182	181
r.m.s. deviations			
bond lengths (Å)	0.006	0.014	0.005
angles (°)	0.89	1.34	0.76
ramachandran			
favored regions/%	99.40	99.41	99.41
allowed regions/%	0.60	0.59	0.59
outliers/%	0.00	0.00	0.00
B-factor (average)	26.44	29.89	27.65
protein	25.12	28.71	25.96
peptide	26.05	31.30	36.25
ligands/ions	40.16	50.33	48.22
water	38.54	40.24	39.81

the NF–YA binding pocket of NF–YB/C, an area of positive (non–modeled) *m*Fo–*D*Fc difference electron density was observed.

Amino acids 270–284 of **5D^N** were successfully built into the electron density (Supporting Figure S9). The C-terminal L285 and the side chain of K284 could not be modeled into the density. Although a residual positive *m*Fo–*D*Fc difference electron density is observed at the C-terminus, we could not build these atoms into our model as they always caused a high negative difference density in accordance with worse refinement statistics. However, the *i,i+4* hydrocarbon staple at positions 272 and 276 could be modeled into the density (Figure 3A).

When comparing NF–YB/C bound **5D^N** (PDB ID 8qu2) with **2D^N** (PDB ID 6qmq) and NF–YA (PDB ID 4awl),[12b,17] we observed the expected very similar binding pose (Figure 3B). Amino acids

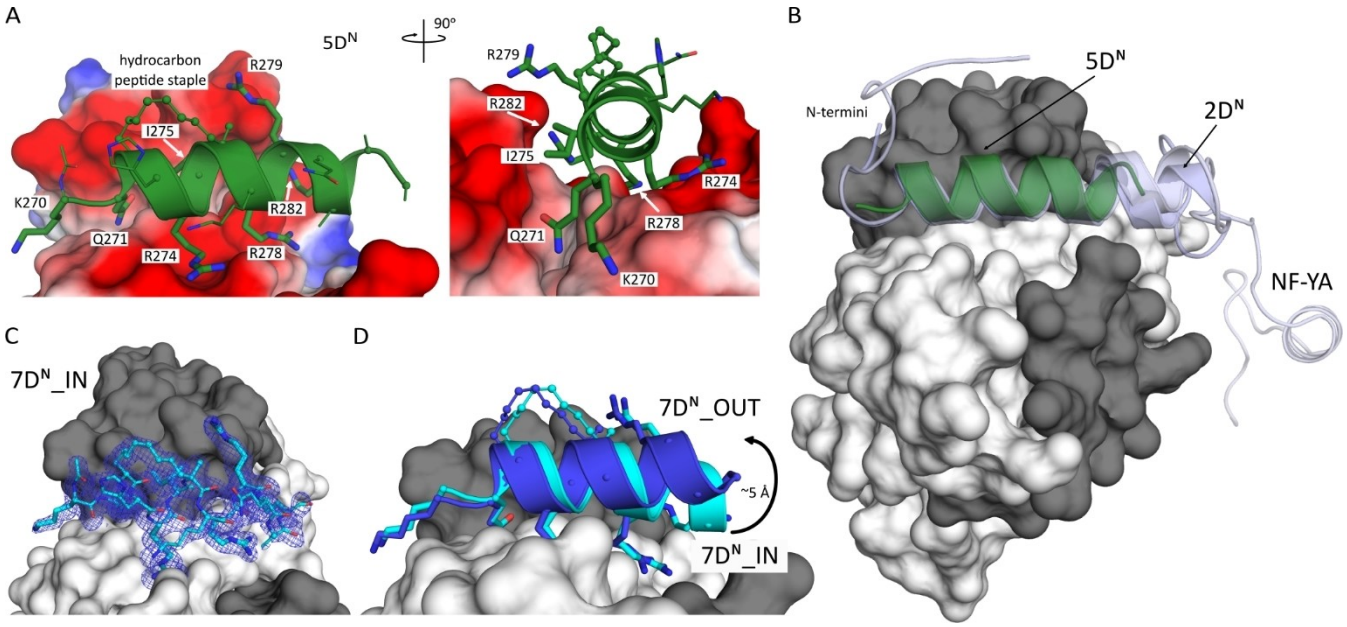

Figure 3. A) Crystal structure of **5D^N** (PDB ID 8qu2, green cartoon and sticks) bound to NF–YB/C (shown as electrostatic surface potential). A 90° rotation of the view reveals the protein interacting amino acids are labeled (shown as thicker sticks). Hydrocarbon peptide staple is indicated. B) Superposition of **5D^N** with **2D^N** and NF-YA (PDB ID 6qmq and 4awl).[12b,17] **5D^N** superimposes with all structures. Longer structures such as **2D^N** or NF–YA show more flexibility at their C-terminal region. C) 2*m*Fo–*D*Fc electron density (contoured at 1 RMSD) of the **7D^N** bound NF–YB/C complex structure with **7D^N** build into the density (light blue sticks) showing the **7D^N**_IN conformation (PDB ID 8qu3). D) Superimposition of **7D^N** in complex with NF–YB/C in its two alternative conformations (PDB ID 8qu3, light blue cartoon and 8qu4, dark blue cartoon) reveals a C-terminal movement out of the binding groove of about 5 Å.

K270, Q271 and the four arginines 274, 278, 279 and 282 form polar and ionic interactions with the negatively charged NF–YB/C surface (Figure 3A). I275 appears to form a weak hydrophobic interaction (distances about 3.5–3.9 Å) towards the π-π-stacked F96 of NF–YB and F113 of NF–YC (Supporting Figure S10). In fact, in the **2D^N** complex structure N268 is the only N-terminal amino acid with an additional side chain contact to NF–YC D109.

In addition, we obtained the crystal structure of the N-terminally further truncated stapled peptide **7D^N** bound to NF–YB/C. At a protein sample concentration of 15 g L^{-1}, the **7D^N** complex crystallized in the same space group as the **5D^N** complex ($P2_12_12_1$, #19). Data up to a resolution of 1.41 Å was used for integration using XDS (Table 1, PDB ID 8qu3). All 13 amino acids comprising **7D^N** (aa 270–282) were successfully built into the observed electron density (Figure 3C). All amino acids involved in interactions, similar to those in **5D^N**, were also observed facilitating the binding of **7D^N** (Supporting Figure S10). To our surprise, a second crystal structure of the **7D^N** complex was obtained utilizing a protein sample concentration of 5 g L^{-1}, however, crystallizing in the same space group as observed before ($P2_12_12_1$, #19), and utilizing data up to a resolution of 1.38 Å (Table 1, PDB ID 8qu4). In this structure, the N-terminal amino acids (aa 270–278) adopted a similar binding pose as observed before (Supporting Figure S10). However, a distinctive divergence was noted in the C-terminal part of **7D^N** (aa 279–282) which displayed a delocalization of about 5 Å and appeared to be shifted out of the binding pocket (7D^N_OUT) when compared to the first structure (7D^N_IN, Figure 3D), thereby R279 gains a polar interaction with S99 of NF–YB, whereas R282 loses side chain contacts to E92 (NF–YB), D116 and I117 (both NF–YC, Supporting Figure S10). These structural variations suggest a flexibility of the C-terminus of **7D^N** in the bound state.

Molecular Dynamics Simulations Confirm Flexibility of 7D^N

To investigate the structural characteristics of the **7D^N**:NF–YB/C complex in more detail, we performed molecular dynamics (MD) simulations starting from the two obtained crystal structures: 7D^N_IN (PDB ID 8qu3) and 7D^N_OUT (PDB ID 8qu4). Five independent simulations for each system were carried out for a cumulated sampling time of 2.5 μs (see methods for details). During each of these simulations, the peptide ligand remained bound to NF–YB/C both starting from for the IN and OUT structure. When analyzing the entire protein/peptide complex, overall only small structural changes were observed, which is reflected in low C_α root mean square deviations (RMSD < 0.2 nm, Supporting Figure S11). In contrast, when focusing only on the bound peptide **7D^N**, the Cα-RMSDs indicated some changes relative to their starting structures (Figure 4A and 4B). Starting simulations from the 7D^N_OUT resulted in relatively small changes in the peptide (Cα–RMSD = 0.14 ± 0.03 nm), while larger conformational changes (Cα–RMSD = 0.29 ± 0.09 nm) were observed when using 7D^N_IN as starting point (Figure 4A). When comparing the peptides from the 7D^N_IN simulations to the 7D^N_OUT crystal structure, we observed a closer overlay (RMSD = 0.17 ± 0.06 nm). This suggests that the peptide of the 7D^N_IN simulations adopted at

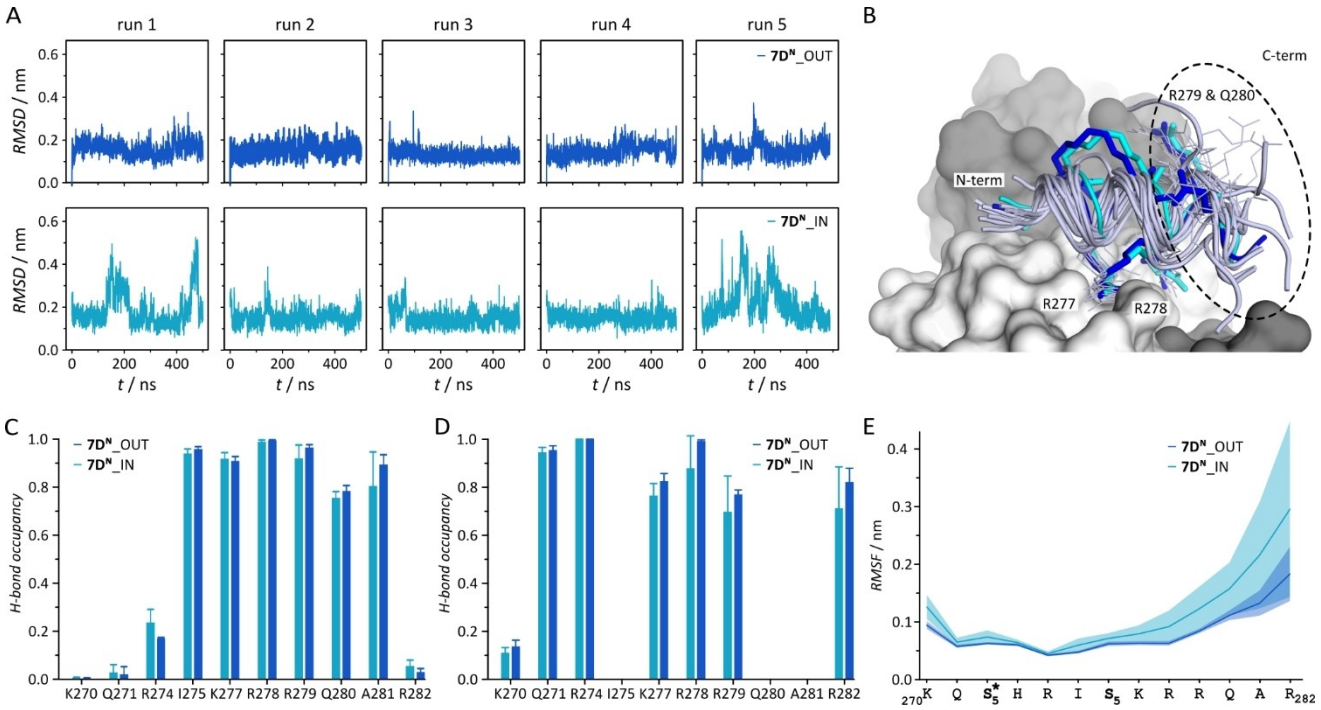

Figure 4. A) Time traces of the root mean square deviation (RMSD) of the Cα-atoms of **7D^N** with respect to the 7D^N_OUT structure over 500 ns. Five MD simulations were performed (run 1–5) starting from the 7DN_OUT crystal structure (PDB ID 8qu4, top panel, dark blue) and from the 7D^N_IN crystal structure (PDB ID 8qu3, bottom panel, light blue). The RMSDs of the peptide are calculated after aligning the complex on chains B and C of the OUT crystal structure to capture the dynamics of the peptide. B) Comparison of 13 snapshots taken every 40 ns of the dynamic trajectory using the 7D^N_IN conformation (PDB ID 8qu3) as a starting point (run 5). According to D) examples of stable residues R277 and R278 are shown as well as flexible residues R279 and Q280 (dashed circle). PDB files of 40 ns snapshots for each run can be found in the supporting information including movies of run 5 snapshots. C) H-bond occupancy within the **7D^N** peptide. The occupancy of a specific hydrogen bond is averaged per system. A hydrogen bond is considered if the donor-H acceptor distance <0.25 nm and for the donor-H acceptor angle $>120°$. The error bars represent the standard error of the mean, calculated as the standard deviation of the average values over the independent runs. The calculation included all the atoms in the system using MDTraj.[21] Light blue: starting model 7D^N_IN, dark blue: starting model 7D^N_OUT. D) H-bond occupancy between **7D^N** and the NF–YB/C heterodimer. E) C_α root mean square fluctuations (RMSF) of **7D^N** in the 7DN_IN (light blue) and 7DN_OUT (dark blue) sets of simulations, after removing overall translation and rotation from the whole complex. The plot shows the RMSF for the peptide. The shaded area indicates the standard deviation of the values calculated over the five independent runs.

least to some extent conformations similar to the 7D^N_OUT structure, indicating a preference for the OUT over the IN conformation.

The preference for conformations similar to 7D^N_OUT is also supported by the hydrogen bond (H-bond) analysis (Figure 4C and 4D) between the peptide and the protein surface, which shows an overall higher H-bond occupancy for 7D^N_OUT conformations when compared to 7D^N_IN conformations. This is particularly relevant in the C-terminal region. **7D^N** forms more often stable H-bonds with the proteins when using 7D^N_OUT as the starting point, as indicated by smaller deviations (Figure 4D). In contrast, we observed larger deviation margins between the C-terminal residues of the peptide when using 7D^N_IN as starting structure, suggesting lower protein engagement for the IN conformation (Figure 4D).

Along these lines, the analysis of the peptide C_α-root mean square fluctuations (RMSF, Figure 4E) indicated that **7D^N** exhibited the highest flexibility in the C-terminal region. The C-terminus can adopt different conformations including 7D^N_OUT and 7D^N_IN arrangements, however, showing a preference for 7D^N_OUT-like conformations (Figure 4B and 4E). To further study the implications of this flexibility, we performed MD simulations for the C-terminally elongated peptide **5D^N** using the above described structure as template (PDB 8qu2, Supporting Figure S12). Again, five independent simulations were carried out for a cumulated sampling time of 2.5 μs (see methods for details). When comparing C_α root mean square fluctuations (RMSF) of the **7D^N** and **5D^N** simulations, we observed similar fluctuation profiles for analogous residues (270–282). The three additional residues in **5D^N** however, exhibited overall the highest flexibility without contributing substantial protein contacts (Supporting Figure 13). Here, it is important to note that **5D^N** ($K_D = 0.8$ μM) shows higher binding affinity than **7D^N** ($K_D = 4.1$ μM) suggesting that this increased flexibility in the bound state contributes to binding. This is a trend that has been reported before and may be explained by a reduced entropic penalty upon binding.[23]

Conclusions

Due to the persistent challenges in targeting transcription factors, there is a demand for tool compounds that can effectively address this challenging class of proteins. Peptides and peptidomimetics emerge as promising candidates, with their potential to be chemically modified for enhanced bio-

logical functions, including increased target affinity and serum stability. This study aimed to understand the impact of miniaturization on the crucial core binding region of a peptidomimetic binder targeting the NF–Y transcription factor. With a high quality NF–YB/C protein complex in hand, our focus was to study the effects of peptide miniaturization on protein binding. As starting point, we used stapled peptide **2D^N** and obtained shorter fragments with reduced yet reasonable binding affinity for NF–YB/C.

Notably, the shorter the fragments were, the more they benefited from stapling (up to 7.3-fold increased stability upon stapling). The structural analysis of truncated peptides **5D^N** and **7D^N** uncovered that both bind to the same NF–YB/C site. Interestingly, we obtained two distinct conformations of the **7D^N** peptide, differing slightly in the arrangement of their C-terminus (IN vs. OUT). MD simulations indicate an increased flexibility of the C-terminal part of the peptide and confirm the accessibility of both crystal structure conformations. Interestingly, the 7D^N_OUT conformation appears to be more preferred, as indicated by a more defined hydrogen bond pattern and a dominant occurrence during MD simulations. In line with this observation, the 7D^N_IN structure appears to relax into the OUT conformation. In essence, this investigation sheds light on the impact of miniaturization on peptide binding to NF–YB/C, unraveling conformational flexibility and offering insights into peptide dynamics through MD simulations Our findings highlights the value simulations can add to the design of bioactive peptides.[22] And, they shed light on the critical role of flexibility in bound peptide ligands, a factor which has been reported to enhance the stability of peptide/protein complexes.[23]

Experimental Section

Full experimental procedures and analytical data can be found in the Supporting Information.

Materials

The reagents and amino acids were purchased from Iris Biotech GmbH (Marktredwitz, Germany), Sigma Aldrich (Darmstadt, Germany), Carl Roth (Karlsruhe, Germany) and unnatural amino acids were purchased from Okeanos Biotech (Beijing, China) and BLD Pharmatech GmbH (Kaiserslautern, Germany).

Solid–Phase Peptide Synthesis

The peptides were synthesized using conventional Fmoc–based solid–phase peptide synthesis, either on an automated peptide synthesizer or by manual peptide synthesis. Initially, the resin was swollen in dimethylformamide (DMF) for 40 min. Reactions were performed at room temperature according to the procedures described in the supporting information. Ring closing metathesis was conducted for macrocyclization of non–natural amino acids using a first generation Grubbs catalyst. For affinity measurements, the final Fmoc deprotected peptides were subsequently labelled with a PEG2 linker and a FITC fluorescent label or alternatively acetylated for crystallization experiments.

Heterologous Protein Expression and Purification

The bacterial expression and purification procedure of NF–YB/C was performed similarly to how it was previously described.[12b] FPLC Ni^{2+}–NTA affinity chromatography followed by tag–cleavage and subsequent Size Exclusion Chromatography (SEC in 25 mM Tris pH 8.0, 1 M NaCl, 1 mM TCEP) was performed for purification. After concentration of pure fractions via ultra–filtration up to 40–70 g L^{-1}, −80 °C.

A detailed description can be found in the supporting information.

Fluorescence Polarization Binding Assay

Prior to the assay, NF–YB/C protein was diluted to a protein-specific start concentration in buffer (25 mM Tris, pH 8.0, 1 M NaCl, 1 mM TCEP). All peptides for FP assays were N-terminally FITC labelled via a PEG2 linker. Peptide stocks in DMSO were diluted in FP buffer (10 mM HEPES pH 7.4, 250 mM NaCl, 0.001 % Tween-20) to a concentration of 40 nM. For the assay, 15 µl of FP buffer was pipetted into each well of a 384-well plate (Corning 384 well microplate). A dilution series with 10 µl of protein solution was performed, and 5 µl of peptide solution was added to each well for a final volume of 20 µl. The final peptide concentration is 10 nM in each well and protein concentrations are 2.4 10^{-4}–1.0 10^{-10} M. The plate was incubated for 1 h on ice. Measurements were performed at 25 °C in a Tecan Spark20 M plate reader (λ_{Ex} = 470 nm; λ_{Em} = 525 nm). Data analysis was performed with GraphPad Prism (version 5.03), and K_D values were determined via a nonlinear regression fit of dose–response curves with variable slope (four parameters).

Thermal Unfolding and Size Analysis

Thermal unfolding profile and dynamic light scattering measurements of NF–YB/C were done by Prometheus NT.48 (NanoTemper GmbH, Munich, Germany). Samples were measured at a protein concentration of 15 µM in buffer containing 25 mM HEPES pH 8.0, 1 M NaCl, 1 mM TCEP. Prior to measurements, the samples were centrifuged for 10 min at 14000 rpm at 4 °C to remove any large aggregates. Single–use glass capillaries were filled with 10–15 µl of the protein sample. For thermal unfolding profile: protein samples were heated at a constant ramp over a temperature range of 35–95 °C with temperature slope of 1 °C min^{-1}. Fluorescence at 330 nm and 350 nm was recorded during the heating process. The DLS size analysis was performed on the same sample (λ_{Ex} = 405 nm). Experimental data analysis was done using the Prometheus Panta Control Software (NanoTemper Technologies).

X-ray Protein Crystallography, Data Collection and Refinement

The purified NF–YB/C heterodimer was dialyzed overnight (Thermo-Scientific Slide–A–Lyzer™ MINI Dialysis Devices, 3.5 K MWCO) into the final crystallization buffer (25 mM Tris pH 8.0, 250 mM NaCl, 1 mM TCEP). Subsequently, the dialyzed protein is mixed with either peptide **5D^N** or **7D^N** (molar ratio of protein : peptide = 1 : 2) and subjected to initial crystallization screening (used sample concentrations: 10, 7.5 and 5.0 g L^{-1}). Crystallization drops were set up using Mosquito (TTP Labtech) by mixing 100 nL of the sample mix and 100 nL of the according reservoir solution. The initial crystallization hits were obtained by using sitting–drop 96-well IQ 3-drop plates (TTP Labtech) at room temperature by screening Morpheus I (Molecular Dimensions) and JCSG I (NeXtal BioTech).

Initial hits of the NF–YB/C:**5D^N** and NF–YB/C:**7D^N** complexes were obtained in Morpheus I[24] G9 (Buffer System 3 (100 mM Bicine/Tris), pH 8.5, Precipitant Mix 1 (PEG 20000:PEG 550 MME 1:2) 30%, Carboxylic Acids (5×200 mM)). Refinement screening involved optimization of the sample mix concentration, the drop size, the pH and the Morpheus Precipitant Mix 1 concentrations in MRC Maxi 48-well plates (Swissci). The best crystals were obtained when an equivalent of 10–15% (v/v) seedstock was added to the sample mix. Therefore, drops with numerous small rod-shaped crystals from previous refinement trials were harvested, harshly mixed and added to the protein:peptide mix.

The best NF–YB/C:**5D^N** slightly thicker rod shaped crystals (~20×30×50 μm) were observed in Buffer System 3 (0.1 M Bicine/Tris), pH 9.0, Precipitant Mix 1 (PEG 20000:PEG 550 MME 1:2) 30%, Carboxylic Acids (5×200 mM) using 15 g L^{-1} sample concentration and formed within 2 days in 880 nL drops. Crystals were fished with LithoLoops (Molecular Dimensions), and were immediately flash–frozen in liquid nitrogen.

The best NF–YB/C:**7D^N** slightly thicker rod shaped crystals (~25×30×60 μm) were observed in Buffer System 3 (0.1 M Bicine/Tris), pH 9.0, Precipitant Mix 1 (PEG 20000:PEG 550 MME 1:2) 24%, Carboxylic Acids (5×200 mM) using 15 g L^{-1} and also 5 g L^{-1} sample concentration and formed within 5 days in drops with a final volume of 880 nL–2.15 μl. Crystals were mounted with 100 μm LithoLoops (Molecular Dimensions). NF–YB/C:**7D^N** crystals were cryo–protected by adding 20% (v/v) glycerol to the reservoir solution and subsequently flash–frozen in liquid nitrogen.

Diffraction data collection was performed on the I04 beamline at the Diamond Light Source (DLS, Didcot, Oxfordshire, UK). Integration of data sets was performed using XDS.[19] Molecular replacement was performed using Phaser[20] MR from the CCP4 software suite[25] (search model:PDB ID 6 qmp, chain B&C only). Iterative cycles of model building and refinement were performed using Coot[26] and Phenix[27] or Refmac 5[28] (Table 1). Images for publication were generated using PyMOL.

Molecular Dynamics Simulations

System Preparation

Three resolved crystal structures were used as starting conformations for the molecular dynamics simulations, *i.e.* 7DN_IN (PDB ID 8qu3), 7DN_OUT (PDB ID 8qu4) and 5DN (PDB ID 8qu2). For 5DN, coordinates were generated for the missing side chain of K284 and L285. The parametrization of the **S_5*** non–natural amino acid relies on existing parameters for its non–methylated analogue nor–leucine, by adding a methyl group to the Cα atom.

Simulation Protocol

All simulations have been carried out using the Gromacs 2020.4 simulation package,[29] the Charmm 36 m forcefield[30] and the TIP3P water model.[31] Three sets of simulations were performed: five 500-ns simulations starting from 7DN_IN, five 500-ns simulations starting from 7DN_OUT and five 500-ns simulations from 5DN, each cumulating to 2.5 μs per complex. For 5DN, the coordinates for L285 and the side chain of K284 were randomly constructed. The atoms in each run were assigned random initial velocities drawn from the Maxwell–Boltzmann distribution at 300 K. The N- and C-termini of the proteins were uncapped, while the peptide was capped with acetyl and NH_2, at its N- and C-terminus, respectively. The side–chains of the histidines were modeled as neutral and protonated at N_δ. The complexes were solvated in periodic dodecahedron boxes, with a minimal distance between the complex and the wall of 1.0 nm. To mimic physiological conditions, 150 mM NaCl ions were added, including neutralizing counterions for the protein complex. The systems were energy minimized following steepest descent prior to a 5-ns NPT equilibration with position restraints on the heavy atoms of the molecules. The temperature and the pressure were maintained at 300 K and 1 atm, respectively, by means of the modified Berendsen thermostat[32] and isotropic Berendsen barostat[33] (0.1 ps coupling and 2 ps coupling, respectively). The production simulations were performed in the NVT ensemble in absence of restraints and with periodic boundary conditions. The short–range interactions were cut off beyond a distance of 1.2 nm, and the potential smoothly decays to zero using the Verlet cutoff scheme. The long–range electrostatic interactions were computed using the Particle Mesh Ewald technique[34] (cubic interpolation order, real space cutoff of 1.2 nm and grid spacing of 0.16 nm) to compute the long-range electrostatic interactions. The bond lengths were constrained by means of a fourth order LINCS algorithm with two iterations.[35] All simulations were run with a time-step of 2 fs and the snapshots were saved every 25 ps.

Supporting Information

Solved crystal structures are deposited in the wwPDB with the PDB accession codes 8qu2, 8qu3, 8qu4. Snapshots from every MD trajectory are extracted every 40 ns and compiled as pdb files for download in the supporting information. Snapshots of run 5 of each starting model are combined in movies 5DN, 7DN_IN and 7DN_OUT. Input files and processed trajectories of the MD simulations are available via figshare: https://doi.org/10.21942/uva.25368475.v1.[36]

Acknowledgements

CD is funded by NWO KLEIN-1 (OCENW.KLEIN.104). I. M. I. acknowledges support from the Sectorplan Beta & Techniek of the Dutch Government and the Dementia Research–Synapsis Foundation Switzerland. Beamline access was provided via the Dutch MX BAG. We thank the user support team as well as the beamline staff of I04 at the Diamond Light Source (Didcot, Oxfordshire, UK) for their support. We thank Dr. Nick Pearce for providing us with the cif consolidate script for proper treatment of crosslinker constrains.

Conflict of Interests

The authors declare no conflict of interest.

Data Availability Statement

Crystal structures will be uploaded into the Protein Data Bank including a doi, but as they are currently "on hold for publication" no doi is available, yet.

Keywords: biophysics · flexibility · peptidomimetic · protein crystallography · protein–protein interaction

[1] a) D. S. Latchman, *The international journal of biochemistry&cell biology* **1997**, *29*, 1305–1312; b) S. Sperling, *BMC Bioinf.* **2007**, *8*, S2; c) P. Weidemüller, M. Kholmatov, E. Petsalaki, J. B. Zaugg, *Proteomics* **2021**, *21*, 2000034.
[2] S. Inukai, K. H. Kock, M. L. Bulyk, *Curr. Opin. Genet. Dev.* **2017**, *43*, 110–119.
[3] J. Das, C.-H. Chen, L. Yang, L. Cohn, P. Ray, A. Ray, *Nat. Immunol.* **2001**, *2*, 45–50.
[4] B. G. Bruneau, *Circ. Res.* **2002**, *90*, 509–519.
[5] B. A. Citron, J. S. Dennis, R. S. Zeitlin, V. Echeverria, *J. Neurosci. Res.* **2008**, *86*, 2499–2504.
[6] M. Sano, T. Minamino, H. Toko, H. Miyauchi, M. Orimo, Y. Qin, H. Akazawa, K. Tateno, Y. Kayama, M. Harada, *Nature* **2007**, *446*, 444–448.
[7] a) M. M. Babu, N. M. Luscombe, L. Aravind, M. Gerstein, S. A. Teichmann, *Curr. Opin. Struct. Biol.* **2004**, *14*, 283–291; b) K. A. Papavassiliou, A. G. Papavassiliou, *J. Cell. Biochem.* **2016**, *117*, 2693–2696.
[8] a) A. Brennan, J. T. Leech, N. M. Kad, J. M. Mason, *JACS Au* **2022**, *2*, 996–1006; b) J. H. Bushweller, *Nat. Rev. Cancer* **2019**, *19*, 611–624; c) M. J. Henley, A. N. Koehler, *Nat. Rev. Drug Discovery* **2021**, *20*, 669–688; d) X. Xie, T. Yu, X. Li, N. Zhang, L. J. Foster, C. Peng, W. Huang, G. He, *Signal Transduction and Targeted Therapy* **2023**, *8*, 335; e) H. Adihou, R. Gopalakrishnan, T. Förster, S. M. Guéret, R. Gasper, S. Geschwindner, C. Carrillo García, H. Karatas, A. V. Pobbati, M. Vazquez-Chantada, *Nat. Commun.* **2020**, *11*, 5425; f) W. S. Horne, T. N. Grossmann, *Nat. Chem.* **2020**, *12*, 331–337; g) L.-G. Milroy, T. N. Grossmann, S. Hennig, L. Brunsveld, C. Ottmann, *Chem. Rev.* **2014**, *114*, 4695–4748.
[9] a) M. Guharoy, P. Chakrabarti, *Bioinformatics* **2007**, *23*, 1909–1918; b) S. Jones, J. M. Thornton, *Progress in biophysics and molecular biology* **1995**, *63*, 31–65; c) M. Pelay-Gimeno, A. Glas, O. Koch, T. N. Grossmann, *Angew. Chem. Int. Ed.* **2015**, *54*, 8896–8927.
[10] J. E. Bock, J. Gavenonis, J. A. Kritzer, *ACS Chem. Biol.* **2013**, *8*, 488–499.
[11] a) C. E. Schafmeister, J. Po, G. L. Verdine, *J. Am. Chem. Soc.* **2000**, *122*, 5891–5892; b) T. N. Grossmann, J. T.-H. Yeh, B. R. Bowman, Q. Chu, R. E. Moellering, G. L. Verdine, *Proc. Natl. Acad. Sci. USA* **2012**, *109*, 17942–17947; c) Y.-W. Kim, T. N. Grossmann, G. L. Verdine, *Nature protocols* **2011**, *6*, 761–771.
[12] a) P. M. Cromm, J. Spiegel, T. N. Grossmann, *ACS Chem. Biol.* **2015**, *10*, 1362–1375; b) S. Jeganathan, M. Wendt, S. Kiehstaller, D. Brancaccio, A. Kuepper, N. Pospiech, A. Carotenuto, E. Novellino, S. Hennig, T. N. Grossmann, *Angew. Chem. Int. Ed.* **2019**, *58*, 17351–17358; c) M. Wendt, *et al., Angewandte Chemie International Edition* **2021**, *60*, 13937–13944.
[13] H. Goodarzi, O. Elemento, S. Tavazoie, *Mol. Cell* **2009**, *36*, 900–911.
[14] a) B. Cao, Y. Zhao, Z. Zhang, H. Li, J. Xing, S. Guo, X. Qiu, S. Zhang, L. Min, S. Zhu, *Int. J. Oncol.* **2018**, *53*, 1857–1868; b) D. Dolfini, V. Andrioletti, R. Mantovani, *Sci. Rep.* **2019**, *9*, 12955.
[15] a) A. Bernardini, M. Lorenzo, M. Nardini, R. Mantovani, N. Gnesutta, *The FASEB Journal* **2019**, *33*, 4790–4801; b) D. Dolfini, F. Zambelli, G. Pavesi, R. Mantovani, *Cell Cycle* **2009**, *8*, 4127–4137; c) V. Nardone, A. Chaves-Sanjuan, M. Nardini, *Biochimica et Biophysica Acta (BBA)-Gene Regulatory Mechanisms* **2017**, *1860*, 571–580; d) C. Romier, F. Cocchiarella, R. Mantovani, D. Moras, *J. Biol. Chem.* **2003**, *278*, 1336–1345.
[16] V. Nardone, A. Chaves-Sanjuan, M. Lapi, C. Airoldi, A. Saponaro, S. Pasqualato, D. Dolfini, C. Camilloni, A. Bernardini, N. Gnesutta, *Cells* **2020**, *9*, 2370.
[17] M. Nardini, N. Gnesutta, G. Donati, R. Gatta, C. Forni, A. Fossati, C. Vonrhein, D. Moras, C. Romier, M. Bolognesi, *Cell* **2013**, *152*, 132–143.
[18] a) S. N. Maity, B. de Crombrugghe, *J. Biol. Chem.* **1992**, *267*, 8286–8292; b) S. Sinha, S. N. Maity, J. Lu, B. De Crombrugghe, *Proc. Natl. Acad. Sci. USA* **1995**, *92*, 1624–1628.
[19] K. W. Xds, *Acta Crystallogr. Sect. D* **2010**, *66*, 125–132.
[20] A. J. McCoy, R. W. Grosse-Kunstleve, P. D. Adams, M. D. Winn, L. C. Storoni, R. J. Read, *J. Appl. Crystallogr.* **2007**, *40*, 658–674.
[21] R. T. McGibbon, K. A. Beauchamp, M. P. Harrigan, C. Klein, J. M. Swails, C. X. Hernández, C. R. Schwantes, L. P. Wang, T. J. Lane, V. S. Pande, *Biophys. J.* **2015**, *109(8)*, 1528–1532.
[22] D. de Raffele, I. M. Ilie, *Chem. Commun.* **2024**, *60*, 632–645.
[23] a) K. Wallraven, F. L. Holmelin, A. Glas, S. Hennig, A. I. Frolov, T. N. Grossmann, *Chem. Sci.* **2020**, *11*, 2269–2276; b) A. Glas, E. C. Wamhoff, D. M. Krüger, C. Rademacher, T. N. Grossmann, *Chemistry–A European Journal* **2017**, *23*, 16157–16161; c) S. Cucuzza, M. Sitnik, S. Jurt, E. Michel, W. Dai, T. Müntener, P. Ernst, D. Häussinger, A. Plückthun, O. Zerbe, *Nat. Commun.* **2023**, *14*, 7823.
[24] F. Gorrec, *J. Appl. Crystallogr.* **2009**, *42*, 1035–1042.
[25] L. Potterton, J. Agirre, C. Ballard, K. Cowtan, E. Dodson, P. R. Evans, H. T. Jenkins, R. Keegan, E. Krissinel, K. Stevenson, *Acta Crystallographica Section D: Structural Biology* **2018**, *74*, 68–84.
[26] P. Emsley, B. Lohkamp, W. G. Scott, K. Cowtan, *Acta Crystallographica Section D: Biological Crystallography* **2010**, *66*, 486–501.
[27] D. Liebschner, P. V. Afonine, M. L. Baker, G. Bunkóczi, V. B. Chen, T. I. Croll, B. Hintze, L.-W. Hung, S. Jain, A. J. McCoy, *Acta Crystallographica Section D: Structural Biology* **2019**, *75*, 861–877.
[28] G. N. Murshudov, P. Skubák, A. A. Lebedev, N. S. Pannu, R. A. Steiner, R. A. Nicholls, M. D. Winn, F. Long, A. A. Vagin, *Acta Crystallographica Section D: Biological Crystallography* **2011**, *67*, 355–367.
[29] a) B. Hess, C. Kutzner, D. Van Der Spoel, E. Lindahl, *J. Chem. Theory Comput.* **2008**, *4*, 435–447; b) H. J. Berendsen, D. van der Spoel, R. van Drunen, *Comput. Phys. Commun.* **1995**, *91*, 43–56.
[30] J. Huang, S. Rauscher, G. Nawrocki, T. Ran, M. Feig, B. L. De Groot, H. Grubmüller, A. D. MacKerell Jr, *Nat. Methods* **2017**, *14*, 71–73.
[31] W. L. Jorgensen, J. Chandrasekhar, J. D. Madura, R. W. Impey, M. L. Klein, *J. Chem. Phys.* **1983**, *79*, 926–935.
[32] G. Bussi, D. Donadio, M. Parrinello, *J. Chem. Phys.* **2007**, *126*.
[33] H. J. Berendsen, J. v Postma, W. F. Van Gunsteren, A. DiNola, J. R. Haak, *J. Chem. Phys.* **1984**, *81*, 3684–3690.
[34] T. Darden, D. York, L. Pedersen, *J. Chem. Phys.* **1993**, *98*, 10089–10092.
[35] B. Hess, H. Bekker, H. J. Berendsen, J. G. Fraaije, *J. Comput. Chem.* **1997**, *18*, 1463–1472.
[36] J. Dataset Vreede, I. M. Ilie, S. Hennig, T. N. Grossmann, C. Bigiotti, *Stapled peptide in complex with transcription factor NF-Y, figshare* **2024**, University of Amsterdam/Amsterdam University of Applied Sciences, https://doi.org/10.21942/uva.25368475.v1.

Manuscript received: January 8, 2024
Revised manuscript received: March 10, 2024
Accepted manuscript online: March 12, 2024
Version of record online: April 2, 2024